Gaussian-type-orbital basis sets for the calculation of continuum properties in molecules: The differential photoionization cross section of molecular nitrogen

Ivo Cacelli*
Scuola Normale Superiore, Piazza dei Cavalieri, I-56100 Pisa, Italy

Roberto Moccia†
Dipartimento di Chimica e Chimica Industriale, Università degli Studi di Pisa, Via Risorgimento 35, I-56126 Pisa, Italy

Antonio Rizzo‡
Istituto di Chimica Quantistica ed Energetica Molecolare del Consiglio Nazionale delle Ricerche, Via Risorgimento 35, I-56126 Pisa, Italy

(Received 6 June 1997; revised manuscript received 8 October 1997)

The differential cross section of the valence one-photon ionization of N_2 is computed in the random phase approximation using large L^2 basis sets of Gaussian-type orbitals (GTO's) and a K-matrix-based technique. Several special polynomial spherical GTO's are included in the basis set used to adequately represent the orbitals lying in the electronic continuum. Ionization channels originating from the $3\sigma_g$, $1\pi_u$, $2\sigma_u$, and $2\sigma_g$ occupied orbitals are considered, both in separated and interacting channel approaches.
[S1050-2947(98)05003-3]

PACS number(s): 33.80.Eh, 33.20.−t, 33.60.−q

I. INTRODUCTION

Molecular nitrogen is a privileged system for studies of molecular photoionization. It has been the subject of a large number of experimental [1–28] and theoretical [29–51] studies. See also Ref. [52].

The system is ideal for both experimentalists, due to the abundance of features in the spectra, and for theorists, who can put their methods and calculations to a severe test.

Valence photoionization of molecular nitrogen has been the subject of analysis of different theoretical groups, and a reference system for different approaches to study the molecular continuum. Early studies by Davenport [32] employed Slater's scattered-wave $X\alpha$ method [53] and could give no account of the details of the spectrum. The Stieltjes-Tchebycheff moments method (SM) [54,55] was employed at different levels of approximation by Rescigno *et al.* and later by Langhoff *et al.* [39] in an analysis of the inner-valence-shell photoionization of molecular nitrogen. The SM in the random phase approximation (RPA) was employed by Williams and Langhoff [40]. Lucchese and co-workers have employed the iterative Schwinger variational method [56,57] in several instances, also recently [41,49–51]. Collins and Schneider have chosen N_2 as one of the systems to which they applied their linear algebraic approach for molecular photoionization [44] and molecular nitrogen has also been the reference taken by Yabushita, McCurdy, and Rescigno to test the efficiency of the complex-basis-function approach in the RPA [48]. Integral photoionization profiles for the valence ionization of N_2 and O_2 were obtained by combining multiconfigurational linear response and SM by Swanström *et al.* [46].

In the last 15 years we have developed a good expertise in the treatment of the properties of the continuum in molecules with L^2 techniques [58–60]. The details of the differential cross section are obtained through a method based upon the determination of the reaction K matrix (KM) in a version adapted to the use of L^2 basis sets [61]. Recently we have devoted our attention to the efficient use of Gaussian-type orbitals (GTO's) as expansion sets for the molecular continuum orbitals. Applications have been made to the photoionization of H_2 [62] and Li_2,LiH [63]. By using a special K-matrix approach, the limitations of GTO's and their inadequacy to describe Coulomb waves at large distances from the origin were overcome. The advantages of the use of GTO's in molecular photoionization are numerous: among others, we mention here the possibility of exploiting computer codes written for the study of bound states, as the multicenter one- and two-electron integral program we developed [64]. Furthermore, expensive one-center expansions of the electronic charge density, Coulomb and exchange potentials can be avoided.

The accurate numerical results reported for N_2 in several papers over the years may then be used as references for different approaches and novel numerical algorithms: it seems only natural to extend our approach to the study of the valence photoionization of the nitrogen molecule. The process of interest is

$$N_2 + h\nu \rightarrow N_2^+ + e^-, \tag{1}$$

with the range of energies extending in the continuum up to 70 eV, well beyond the inner-valence ionization threshold, e.g., for the photoejection of electrons from the four valence molecular orbitals ($3\sigma_g$, $1\pi_u$, $2\sigma_u$, and $2\sigma_g$).

*Author to whom correspondence should be addressed. Electronic address: ivo@hal.icqem.pi.cnr.it
†Electronic address: rob@ibm355.icqem.pi.cnr.it
‡Electronic address: rizzo@hal.icqem.pi.cnr.it

In the following, after a brief review of the theory and a description of the computational tools, a detailed account of the features of the differential photoionization cross section profile of N_2 will be given.

II. THEORY

Our method to obtain the states into the continuum may be considered a configuration interaction approach where the multielectron basis, formally, includes the one-electron continuum. The diagonalization of the resulting energy matrix [65] is equivalent to the solution of the system of integral equations for the half-on-the-shell reaction K matrix. To ascertain the equivalence let us assume that for each symmetry Γ, the multielectron basis comprises the following.

(i) Several partial wave channel (PWC) sets of functions $|\Phi_{\gamma,E}\rangle$ built as products of well defined localized ion states (target states) $|\Phi^{N-1}_{E_I,S_I,\Gamma_I}\rangle$ times very diffuse orbitals $\varphi_{l,m,\epsilon}$ to represent the one-electron continuum. The products are coupled to give the correct symmetry Γ and spin multiplicity S; a greek index is employed to specify all labels, i.e., $\gamma \equiv E_{I_\gamma}, S_{I_\gamma}, l_\gamma, m_\gamma, S_\gamma$ where $E = E_{I_\gamma} + \epsilon$.

(ii) A localized channel (LC) set of functions $|\Phi_{C,E_j}\rangle$, linear combination of Slater determinants built from a set of localized (short-range) orbitals.

These multielectron basis functions are chosen such as to diagonalize the electronic molecular Hamiltonian separately for each channel and for each ion state considered, i.e.,

$$\langle\Phi_{C,E_j}|\hat{H}|\Phi_{C,E_k}\rangle = \delta_{j,k}E_j, \quad \langle\Phi_{C,E_j}|\Phi_{C,E_k}\rangle = \delta_{j,k}, \quad (2)$$

$$\langle\Phi_{\beta,E''}|\hat{H}|\Phi_{\beta,E'}\rangle = \delta_{E'',E'}E'', \quad \langle\Phi_{\beta,E''}|\Phi_{\beta,E'}\rangle = \delta_{E'',E'}, \quad (3)$$

$$\langle\Phi^{N-1}_{I'}|\hat{H}^{N-1}|\Phi^{N-1}_{I}\rangle = \delta_{I',I}E_I, \quad \langle\Phi^{N-1}_{I'}|\Phi^{N-1}_{I}\rangle = \delta_{I',I}. \quad (4)$$

It should be emphasized that both continuum and discrete states occur in the PWC's. Thus the $\delta_{E'',E'}$ stands both for a Dirac $\delta(E''-E')$ in the continuum and a Kronecker symbol in the discrete part of the spectrum. Since the solutions of Eq. (3) are by construction $|\Phi_{\beta,E'}\rangle = |\Phi^{N-1}_{I_\beta}\varphi_{l_{\beta,m_{\beta,\epsilon}}}\rangle$, they determine the best one-electron PWC continuum orbitals $\varphi_{l_{\beta,m_{\beta,\epsilon}}}$ for a given parent ion $|\Phi^{N-1}_{I_\beta}\rangle$. It should also be obvious that, by this procedure, the multielectron basis functions belonging to different channels of the same manifold are not orthogonal, i.e., for

$$\theta \neq \gamma, \quad \langle\Phi_{\theta,E''}|\Phi_{\gamma,E'}\rangle \neq 0, \quad \langle\Phi_{\theta,E''}|\hat{H}|\Phi_{\gamma,E'}\rangle \neq 0. \quad (5)$$

Thus the matrix elements $V_{\theta E'',\gamma E'}(E)$ may be defined by

$$\langle\Phi_{\theta,E''}|\hat{H}-E|\Phi_{\gamma,E'}\rangle = \delta_{\theta,\gamma}\delta_{E'',E'}(E''-E) + V_{\theta E'',\gamma E'}(E). \quad (6)$$

Employing this basis, the stationary states in the continuum may be expressed as

$$|\Psi_{\beta,E}\rangle = |\Phi_{\beta,E}\rangle + \sum_\gamma \int\!\!\!\!\!\!\diagup dE' |\Phi_{\gamma,E'}\rangle \mathrm{P}\frac{1}{E-E'} K_{\gamma E',\beta E}, \quad (7)$$

where the $\int\!\!\!\!\!\!\diagup$ stands for summation upon the discrete states and integration upon the energy in the continuum and where the sum upon the channels includes, besides all PWC's, also the LC. The requirement

$$\langle\Phi_{\theta,E''}|\hat{H}-E|\Psi_{\beta,E}\rangle = 0, \quad \forall\,\theta,E'', \quad (8)$$

which is tantamount to diagonalizing the total Hamiltonian matrix with continuous indices as in a standard time-honored variational calculation proposed by Fano [65], yields the system of integral equations for the $K_{\gamma E',\beta E}$ coefficients, which may be recognized as the elements of the half-on-the-shell K matrix

$$\sum_\gamma \int\!\!\!\!\!\!\diagup dE' \left\{ \delta_{\theta,\gamma}\delta_{E'',E'} - V_{\theta E'',\gamma E'}\mathrm{P}\frac{1}{E-E'} \right\} K_{\gamma E',\beta E} = V_{\theta E'',\beta E}. \quad (9)$$

On the other hand, it should be pointed out that Eqs. (9) also represent the stationary value of the functional

$$\begin{aligned} I(E,\alpha,\beta) = {} & \sum_\gamma \int\!\!\!\!\!\!\diagup dE' \left[K_{\alpha E,\gamma E'}\mathrm{P}\frac{1}{E-E'} V_{\gamma E',\beta E} + V_{\alpha E,\gamma E'}\mathrm{P}\frac{1}{E-E'} K_{\gamma E',\beta E} \right] \\ & + \sum_\gamma \int\!\!\!\!\!\!\diagup dE' K_{\alpha E\cdot\gamma E'}\mathrm{P}\frac{1}{E-E'} \left[K_{\gamma E',\beta E} + \sum_\theta \int\!\!\!\!\!\!\diagup dE'' V_{\gamma E',\theta E''}\mathrm{P}\frac{1}{E-E''} K_{\theta E'',\beta E} \right] \\ & + V_{\alpha E,\beta E}, \end{aligned} \quad (10)$$

for arbitrary variations of the $K_{\gamma E',\beta E}$'s. Thus, since for the $K_{\gamma E',\beta E}$ satisfying Eqs. (9) the functionals $I(E,\alpha,\beta)$ are equal to the $K_{\alpha E,\beta E}$, it turns out that the resulting K matrix on the shell is stationary.

The K matrix and the S matrix are connected by the well known relations

$$\mathbf{S}(E) = \frac{\mathbf{1} - i\pi\mathbf{K}(E)}{\mathbf{1} + i\pi\mathbf{K}(E)},$$

where $\mathbf{K}(E)$ is the matrix upon the energy shell. The states which satisfy the boundary condition appropriate for a photoionization process are given by

$$|\Psi^{(-)}_{\beta,E}\rangle = \sum_\gamma |\Psi_{\gamma,E}\rangle [\mathbf{1} - i\pi\mathbf{K}(E)]^{-1}_{\gamma,\alpha}. \quad (11)$$

The positions and the widths of the autoionizing states may then be found by looking for the zeros of $\mathbf{1} + i\pi\mathbf{K}(E)$ via analytical continuation.

The use of L^2 orbitals implies that our multielectron basis functions cannot yield the true continuum. Therefore the system of integral equations (9) is discretized using as grid points the energy values provided by separate channel variational calculations, according to Eqs. (2)–(4) [59].

An important point for the success of the method is the knowledge of the additional phase shifts $\delta(k)$ of the orbitals $\varphi_{l,m,\epsilon}$, needed to evaluate the asymmetry parameters. With the use of suitable polynomial spherical GTO's (PSGTO) to represent such orbitals these quantities were achieved by a special technique already described elsewhere [63].

It is worthwhile to emphasize that the $V_{\theta E'',\gamma E'}(E)$ matrix elements are evaluated without making any approximation for the lack of orthogonality among different channels. Their exact evaluation, together with the presence of the LC, is quite important, since they account properly for the correct behavior of the continuum states in the molecular region. This makes the use of high values of l, which seems mandatory in other methods [66,50], unnecessary. The feature is extremely convenient from a computational viewpoint.

A K-matrix-like approach may also be implemented within the RPA framework. In fact by employing excitation operators corresponding to the unoccupied self-consistent field (SCF) orbitals for the LC, and to the orbitals $\varphi_{l_\gamma,m_{\gamma,\epsilon}}$ for the PWC's, it is possible to set up the RPA scheme. The resulting equations

$$\begin{pmatrix} \mathbf{M} & \mathbf{Q} \\ \mathbf{Q}^* & \mathbf{M}^* \end{pmatrix} \begin{pmatrix} \mathbf{X}_{\cdot,\alpha E} \\ \mathbf{Y}_{\cdot,\alpha E} \end{pmatrix} = E \begin{pmatrix} \mathbf{S} & \mathbf{0} \\ \mathbf{0} & -\mathbf{S}^* \end{pmatrix} \begin{pmatrix} \mathbf{X}_{\cdot,\alpha E} \\ \mathbf{Y}_{\cdot,\alpha E} \end{pmatrix} \tag{12}$$

refer now to a basis which formally includes excitations into the continuum. In the RPA the ion states are characterized simply by the j_γ index of the emptied SCF orbital. The normalization becomes

$$\mathbf{X}^\dagger{}_{\cdot,\beta E'}\mathbf{S}\mathbf{X}_{\cdot,\alpha E} - \mathbf{Y}^\dagger{}_{\cdot,E'\beta}\mathbf{S}^*\mathbf{Y}_{\cdot,\alpha E} = \delta_{E',E}\delta_{\alpha,\beta}, \tag{13}$$

where E indicates the excitation energies with respect to the ground state SCF energy. Due to the lack of orthogonality among the orbitals of different channels, the matrices **M** and **Q** are not the usual RPA matrices. The detailed expressions of the elements of the **M**, **Q**, **S** matrices may be found in [67].

For energies corresponding to excitation in the continuum Eq. (12) above is solved by posing

$$\mathbf{X}_{\beta E',\alpha E} = \delta_{\alpha\beta}\delta_{E',E} + \mathrm{P}\,\frac{1}{E-\epsilon}\,\mathbf{K}_{\beta E',\alpha E}, \tag{14}$$

$$\mathbf{Y}_{\beta E',\alpha E} = \mathbf{L}_{\beta E',\alpha E}. \tag{15}$$

This yields a system of integral equations for the **K** and the **L** matrices. The numerical implementation of the RPA with L^2 basis follows closely the procedure described above. Thus, by using as grid points those provided by the L^2 basis set calculation and exploiting adequate quadrature formulas, the system of integral equations reduces to a system of linear equations which may be solved for arbitrary values of the excitation energy. The one-electron transition densities $\rho_{0,\beta E}$ yielded directly by the solution of the RPA equations are then transformed to obtain the transition densities appropriate to photoionization according to

$$\rho^{(-)}_{0,\alpha E} = \sum_\beta \rho_{0,\beta E}[\mathbf{1} - \imath\pi\mathbf{K}(E)]^{-1}_{\beta,\alpha}, \tag{16}$$

were as usual $\mathbf{K}(E)$ is the on-the-shell RPA K matrix.

TABLE I. Ionization potentials of the four outer orbitals of molecular nitrogen (eV).

Ion state Orbital	$X\ ^2\Sigma_g^+$ $3\sigma_g$	$A\ ^2\Pi_u$ $1\pi_u$	$B\ ^2\Sigma_u^+$ $2\sigma_u$	$^2\Sigma_g^+$ $2\sigma_g$
Koopman's	17.19	16.70	21.12	40.19
Experiment[a]	15.57	≈ 17.0[b]	18.75	≈ 38[c]

[a]From Ref. [70]. See also Ref. [68].
[b]Taken as the approximate centroid of the Franck-Condon band.
[c]Taken as the approximate centroid of the several ionization thresholds for the ion states lying in the region.

III. COMPUTATIONAL DETAILS

In the dipole, vertical transition approximation for random molecular orientation, the orientational averaged differential cross section for the transition from the initial state $|\Psi_0\rangle$ to a continuum final state $|\Psi^{(-)}_{j_\beta,E',\hat{k}}\rangle$, due to the absorption of one photon of energy ω, can be expressed as [59] (a.u.)

$$\frac{d\sigma_{j_\gamma}(\omega)}{d\hat{k}} = \frac{\sigma_{j_\gamma}(\omega)}{4\pi}\,[1+\beta_{j_\gamma}P_2(\cos\,\theta)], \tag{17}$$

where $\sigma_{j_\gamma}(\omega)$ is the integral cross section and β the asymmetry parameter. The index j_γ collects all the labels identifying the asymptotic parent ion state $|\Psi^{N-1}_{j_\gamma}\rangle$ which is spin coupled to the continuum orbital $|\varphi_{\epsilon\hat{k}}\rangle$ describing the electron emitted with energy $\epsilon = E' - E^{N-1}_{j_\gamma}$ in the direction $\hat{k}$. θ is the angle between the photon polarization and k. The states $|\Psi^{(-)}_{j_{\gamma,E',\hat{k}}}\rangle$ are obtained by the standard procedure as a linear combination of the PWC's $|\Psi^{(-)}_{\beta,E}\rangle$ of Eq. (11): for the RPA corresponding linear combinations of the transition densities, Eq. (16), are used. The calculations were performed both within the static-exchange approximation (SEA) and RPA frameworks. In the present study only the RPA results are reported since they were found to be always of superior quality both in comparison with experiments and as regards the gauge agreement. The computational scheme was outlined in Ref. [63].

The experimental equilibrium geometry ($R = 2.068$ Å) was adopted [68]. The molecule was placed along the z axis. The reference ground state of the neutral molecule was described at the SCF level employing a basis set derived from Pople's 6-31G* set [69] with the second s and inner p functions decontracted, and the exponent of the d function variationally determined ($\xi = 0.95$). The ground state energy was $E_{\mathrm{SCF}} = -108.946\,74$ a.u. Excitations involving all four valence orbitals were all included in the calculations. In Table I the corresponding ionization potentials (IP's) as provided by SCF in the Koopman approximation are compared with experiment [68,70]. It is well known that Koopman's theorem is unable to reproduce the correct order of the valence orbitals of molecular nitrogen. The highest occupied molecular orbital is predicted to be the $1\pi_u$ instead of the $3\sigma_g$. The three lower lying ionization channels open within about 3 eV. Thus the low lying spectral region is characterized by several Feshbach-type resonances, in particular where the Hopfield autoionizing states lie [71]. In order to get a better

TABLE II. Spherical partial waves (l,m) included in the calculation, with the excitations to which they contribute. $l_{max}=7$. Only the components with $m>0$ are indicated.

Excitation		Spherical waves	Total number of PWC's
$2\sigma_g$, $3\sigma_g$	$\rightarrow k\sigma_u(^1\Sigma_u^+)$	(10), (30), (50), (70)	4(+4)
	$\rightarrow k\pi_u(^1\Pi_u)$	(11), (31), (51), (71)	4(+4)
$1\pi_u$	$\rightarrow k\sigma_g(^1\Pi_u)$	(00), (20), (40), (60)	4
	$\rightarrow k\delta_g(^1\Pi_u)$	(22), (42), (62)	3
	$\rightarrow k\pi_g(^1\Sigma_u^+)$	(21), (41), (61)	3
$2\sigma_u$	$\rightarrow k\sigma_g(^1\Sigma_u^+)$	(00), (20), (40), (60)	4
	$\rightarrow k\pi_g(^1\Pi_u)$	(21), (41), (61)	3

description of this part of the spectrum the computed IP's have been replaced by the experimental ones.

The orbitals employed to describe the PWC's were expanded on PSGTO's for l up to 3 and usual spherical GTO's in geometrical sequences for $l>3$. In Ref. [63] PSGTO's were proven to be particularly efficient to expand low-l PWC's, due to the strong attractive characteristics of the molecular potential. The maximum value of l was here 7. All PWC's were centered at the midpoint of the molecular axis. Table II shows how the spherical components contribute to the PWC's; see Refs. [72,73] for details. A total of 15 PWC's for the $^1\Sigma_u^+$ final state symmetry, and of 18 PWC's for each component of the $^1\Pi_u$ final state symmetry entered the calculations.

The PWC orbitals for a given j, l, m were determined by solving the one-electron problem yielded by the SEA effective Hamiltonian

$$\hat{h}_{j,\mathrm{SEA}}=\hat{T}+\hat{V}_{j,\mathrm{SEA}}^{N-1}, \tag{18}$$

where the last term represents the effective SEA potential for the j hole. No orthogonality constraints were imposed. Incidentally we note that in order to obtain zero-order states of definite spatial symmetry, special effective Hamiltonian operators are to be introduced when the orbital j belongs to a two-dimensional irreducible representation [72].

The LC includes excitations to the virtual SCF orbitals and to a few tight functions with $l=0$, 1, and 2. These last functions are introduced to give a better description of the behavior of the final one-electron continuum states near the nuclei, where the potential dip localizes some electron density. The LC orbitals are orthogonal by construction to the occupied SCF orbitals.

Due to the overlap of the partial wave orbitals and the localized orbitals in each channel, the complete basis set, including the several PWC's and the LC, is highly redundant. Moreover, it has been mentioned above that the PWC orbitals are not orthogonal to the occupied molecular orbitals. Since the K-matrix technique involves numerical integrations which become especially delicate when using redundant expansion sets, the nonorthogonality may lead to anomalies and spurious results.

To deal adequately with this problem, the following transformations of the basis set were performed.

(1) For each channel, the LC orbitals and the portion of the PWC orbitals lying in the discrete are orthogonalized simultaneously to the remaining PWC orbitals (lying in the true continuum) and to the occupied molecular orbitals (MO's). The **M** matrix in this space is then diagonalized using the metric orthogonalization, discarding the metric eigenvectors with a norm lower than a given threshold. This minimizes the redundancy of the basis, and the overlap between the SCF occupied orbitals and the excited (discrete and continuum) orbitals.

(2) The solution of the K-matrix equation is obtained using the metric matrix, as described in Ref. [74].

This procedure can in principle give rise to a sort of ''intruder'' states, e.g., localized wave packets that fall in the energy range spanned by the true continuum PWC's. They could produce unphysical Feshbach-type resonances, but are not influential in the present case, their linewidth being quite large and their effect being thus smoothly spread over a wide energy range.

The cross sections and the asymmetry parameters were convoluted with a Gaussian function with full width at half maximum (FWHM) of 0.5 eV, a value chosen as a compromise between the Franck-Condon amplitudes of the three low lying ion states and the spectral resolution of the available experimental data.

IV. RESULTS AND DISCUSSION

A. Total cross section

The integral photoionization cross section for the process (1) computed in the KM RPA using PWC's with l up to 7, is shown in Fig. 1. The four curves correspond to the results of our investigation in both the interacting channels (IC) and single channel (SC) approximations and in the length gauge (LG) and velocity gauge (VG) choices of the interaction operator.

The two sets of experimental data of Samson *et al.* [9] in the lower part of Fig. 1 show convincingly that decay patterns other than ionization are negligible for photon energies greater than 19 eV [6], where photoionization and photoabsorption probabilities are practically the same. For lower photon energies our data, obtained at a fixed geometry, should be properly compared with photoabsorption data.

The band at 16 eV in the IC approximation arises from $1\pi_u$ Feshbach resonances that are smoothed out in the $3\sigma_g$ continuum, appearing as a single large band after convolution of the spectrum. This band does not appear in the SC calculation, since the contributions of the discrete states in each channel are ignored.

It is immediately apparent from the figures that both the gauge agreement and the agreement with experiment for the total cross section are greatly enhanced by the introduction of the interaction between the ionization channels.

A common feature observed for all PWC's is that multichannel effects on the observables are stronger in the $^1\Sigma_u^+$ than in the $^1\Pi_u$ final state symmetry. A likely explanation is that the effect of the IC is felt more by the transition moment parallel to the molecular axis than by the perpendicular components, since the former is more sensible to the details of the wave function near the nuclei. This does not necessarily imply that, from the energy viewpoint, the $^1\Sigma_u^+$ final states feel the effects of the channel mixing more than the others.

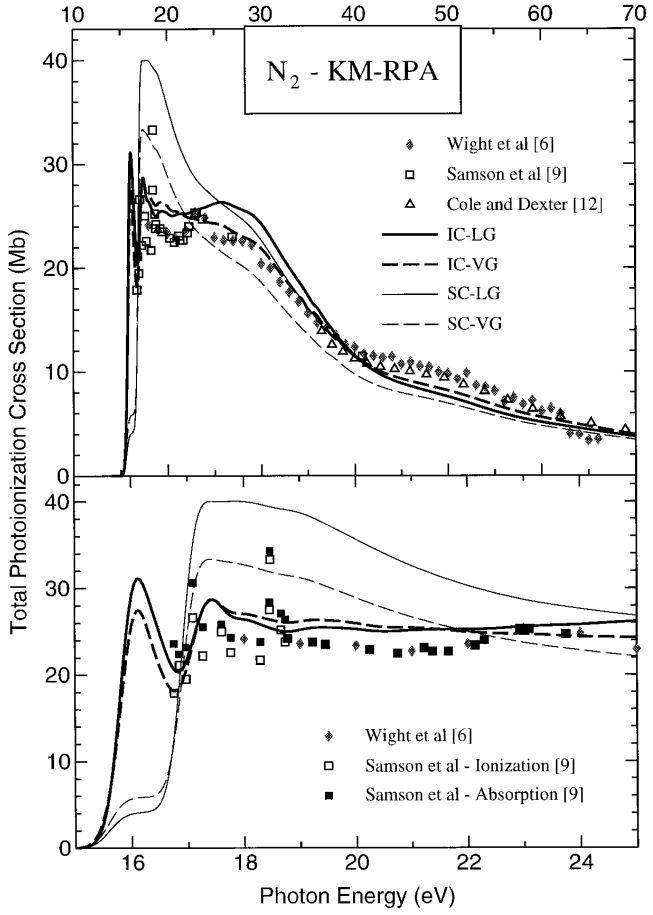

FIG. 1. The total photoionization cross section of N_2 (Mb) in the 10–70-eV photon energy range (above) and an enlargement of the 15–25-eV portion of the spectrum (below). IC: Interacting channels; SC: single channel; LG: length gauge for the interaction operator; VG: velocity gauge for the interacting operator. Also reported are some sets of experimental data. In all figures the theoretical *K*-matrix results are convoluted with a normalized Gaussian function with FWHM of 0.5 eV.

The SEA results show a very large gauge disagreement in the whole energy spectrum. For instance in the 18–24 eV energy range the LG cross section is 33 Mb on the average, e.g., about twice the VG estimate. For higher photon energies the ratio is nearly constant and the VG and LG results bracket both the experimental and RPA results.

B. Partial wave expansion and effect of the localized channel

A check of the convergence in the (l,m) expansion of the PWC's and on the effects of the LC was performed by comparing three sets of results, corresponding to the following calculations: $C1$—$l_{\max}=7$; LC included; $C2$—$l_{\max}=5$; LC included; $C3$—$l_{\max}=7$; LC absent.

The differences between the results of $C1$ and $C2$ are very limited. In the 15–20-eV energy range the total cross section for $C1$ is larger than that for $C2$ by 1.0 to 1.5 Mb. At higher photon energies this difference lowers to a fraction of Mb in the LG, while the results obtained in the VG are practically the same. Contributions to the velocity gauge come mainly from the spatial regions close to the nuclei, where higher angular moment waves assume smaller values due to the repulsion effects of the centrifugal potential. This leads to the conclusion that VG should exhibit faster convergence with the angular expansion than LG. Note, however, that—independent of the gauge—some effects of waves not included in the PWC expansion are taken properly into account with the inclusion of the localized channel. This makes the l convergence faster (see Ref. [63] for a detailed discussion).

The LC appears to have sensible effects in the low energy region ($E<22$ eV) both for SC and IC. Excluding it, as in $C3$, leads to an increase of the total cross section by about 3–4 Mb on the average in the 18–22-eV energy range, and to a lowering of about 4 Mb of the first peak located around 16 eV. This transfer of intensity is mainly due to the spread of the $1\pi_g^*$ antibonding orbital in the discrete and continuum regions of the $1\pi_u \rightarrow (l=2,m=1)(\pi_g)(^1\Sigma_u^+)$ partial channel induced by the noticeable interaction with other channels. Thus the exclusion of the LC increases the discrepancies with experiment and leads to a general worsening of the gauge agreement.

As expected, the effects of the LC are more evident in the LG, which proves to be more sensible to the quality of the wave function near the nuclei. Indeed, the LC orbitals are important for a better description of the behavior of the wave function near the off-center nuclei. As discussed in Ref. [63], this is more effective in the LG than in the VG. For N_2, however, the effects are much less pronounced than those found in Li_2 [63], the reason being most probably the shorter bond distance of N_2.

C. Photoionization from the $3\sigma_g$

Figure 2 shows the cross section and the asymmetry parameter for the partial photoionization channel involving the $3\sigma_g$ orbital, e.g., leading to the $X\ ^2\Sigma_g^+$ ion state. Together with the computed IC and SC curves (shown for both LG and VG), some experimental reference data are displayed.

As noted before, the very intense peak around 16 eV, seen by Samson, Haddad, and Gardner [9], arises from Feshbach resonances converging to the $1\pi_u$ threshold and embedded in the $3\sigma_g$ continuum in the IC picture.

The major feature in Fig. 2 is the large shape resonance appearing at a photon energy of about 30 eV. Both the SC and IC approximation can reproduce this largely monoelectronic resonance, which is essentially due to the $3\sigma_g \rightarrow 3\sigma_u^*$ molecular excitation or, in the PWC ''language,'' to $3\sigma_g \rightarrow (3,0)$ transitions. In this region and up to 40 eV the single channel approximation performs distinctly better than the multichannel approximation. An analogous observation was made by Lucchese and Zurales in Ref. [50], and it appears that the hypothesis put forward by these authors, e.g., that the neat increase in the partial cross section in the multichannel approximation might be due to the interaction with the $1\pi_u$ ionization channel, can be confirmed. Indeed we performed a test calculation involving only the $3\sigma_g$ and the $2\sigma_u$ channels and observed only a small increase of the $3\sigma_g$ partial photoionization cross section with respect to the SC calculation.

Two possible explanations for this behavior have been discussed in the literature. The first one is based upon evi-

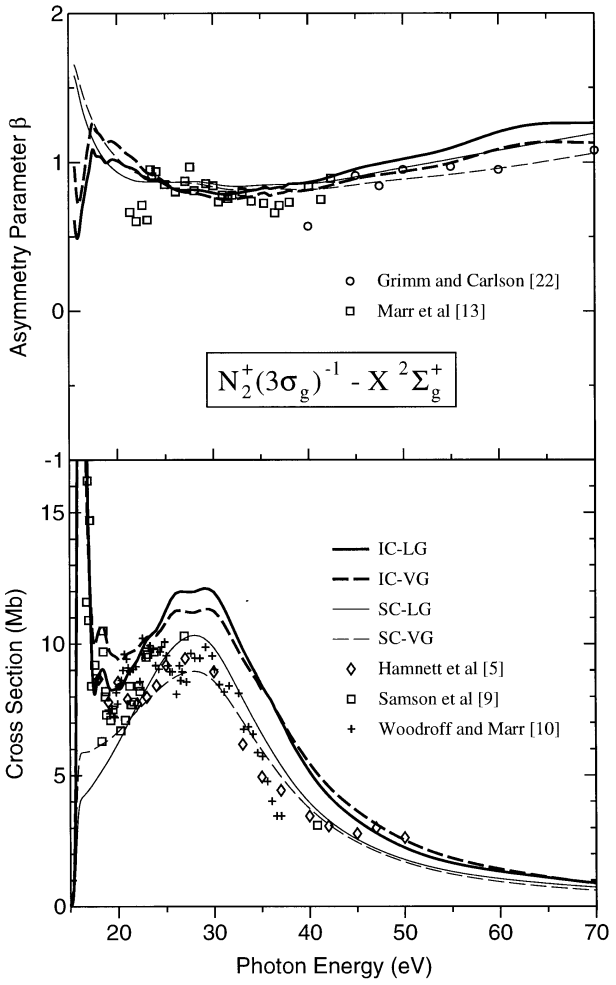

FIG. 2. Partial cross section (Mb) and asymmetry parameter β for the photoionization leading to the $N_2^+(3\sigma_g)^{-1}X\ ^2\Sigma_g^+$ state in the 15–70-eV photon energy range. See caption to Fig. 1.

dences of the existence of multiply excited states producing peaks in the 29-eV region of the excitation spectrum [75,5, 18,21,39]. Although the interaction between these multiply (mainly doubly) excited states and those coming from excitations out of the $3\sigma_g$ orbital is expected to be weak, some transfer of oscillator strength might lead to a decrease of the $3\sigma_g$ partial cross section in a relatively small energy region. Thus the inclusion of doubly excited states in the configurational space could improve the agreement between theory and experiment.

A second possible cause for the enhancement of the cross section due to the $3\sigma_g$, $1\pi_u$ interaction might be the extension (more than 1 eV) of the Franck-Condon structure of the $A(^2\Pi_u)$ band in the photoelectron spectrum [70]. The results of the two-channel calculations ($3\sigma_g$, $2\sigma_u$) of Basden and Lucchese [49], although not yet in quantitative agreement with experiment, show the dramatic effects of the internuclear separation on the partial cross section, which shift the shape resonance in the 25–35 eV region, and the strong enhancement in the $3\sigma_g$ spectrum, coupled to a corresponding decrease of intensity in the $2\sigma_u$ spectrum induced by the channel interaction.

As far as the angular distribution of the photoelectrons in the $3\sigma_g$ channel is concerned, there are no striking differ-

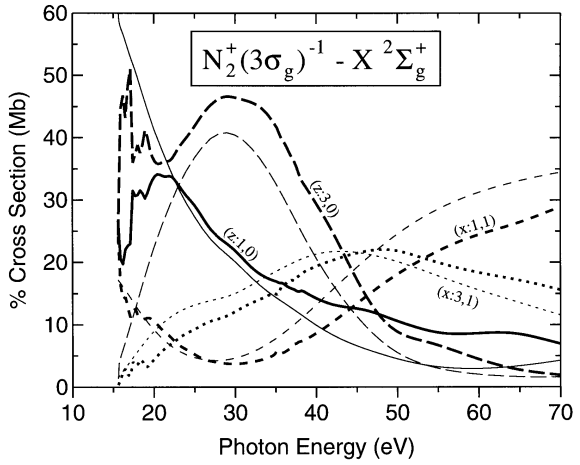

FIG. 3. Relative contribution of the individual partial wave channels to the photoionization leading to the $N_2^+(3\sigma_g)^{-1}X\ ^2\Sigma_g^+$ state. The labels x and z indicate the dipole transition operators and also the final state spatial symmetry. Only the symmetry-independent contributions are reported. Thick lines: IC approximation. Thin lines: SC approximation.

ences between the SC and IC approaches, except for the low energy region ($E<18$ eV), where a complex resonant pattern resulting from the channel interaction appears. This behavior may be explained with the help of Fig. 3, where the relative contributions to the cross section from the more important PWC's is shown for both the SC and IC approximations.

In the low energy range the SC cross section is given practically by the p waves alone. The predominance of waves with small values of l at low photon energies is due to the effects of the centrifugal potential. High-l waves are thus much less ''penetrating'' than low-l waves at low photon energies [63]. Introducing the channel coupling, the interaction of waves of different energies and belonging to a different ion state may cause a transfer of oscillator strength between waves. This may lead to significant contributions of waves with high-l quantum number. In Fig. 3 the large variation in the percentage contribution of the (1,0) and (3,0) waves seen going from SC to IC around 16 eV is mainly due to the interaction with the discrete part of the $1\pi_u$ channel ($^1\Sigma_u^+$ symmetry) and it is responsible for the different behavior of β_{SC} and β_{IC} in that region.

Figure 3 also shows that for high photon energies, where $\beta_{SC} \lesssim \beta_{IC}$, the $3\sigma_g \rightarrow k\pi_u$—in particular the $3\sigma_g \rightarrow k(1,1)\pi_u$—PWC dominates, especially in the SC. Moreover, the importance of the $3\sigma_g \rightarrow k(1,0)\sigma_u$ PWC increases in the IC approach, the relative weight of the (1,1) and (1,0) waves being roughly 3:1 in the SC and 2:1 in the IC. This partly explains the enhancement of the asymmetry parameter observed in the IC approach at large photon energies.

The agreement of the asymmetry parameter with experiment is in general fairly good. Note that the broad valley around 22 eV in the experiment [13,23] has been shown to be due to a doubly excited state of $(1\pi_u)^{-1}(3\sigma_g)^{-1}(1\pi_g)^1\ ^2\Sigma_u^+$ dominant ionic configuration [51]. States of this type are not considered in our approximation. See also [51].

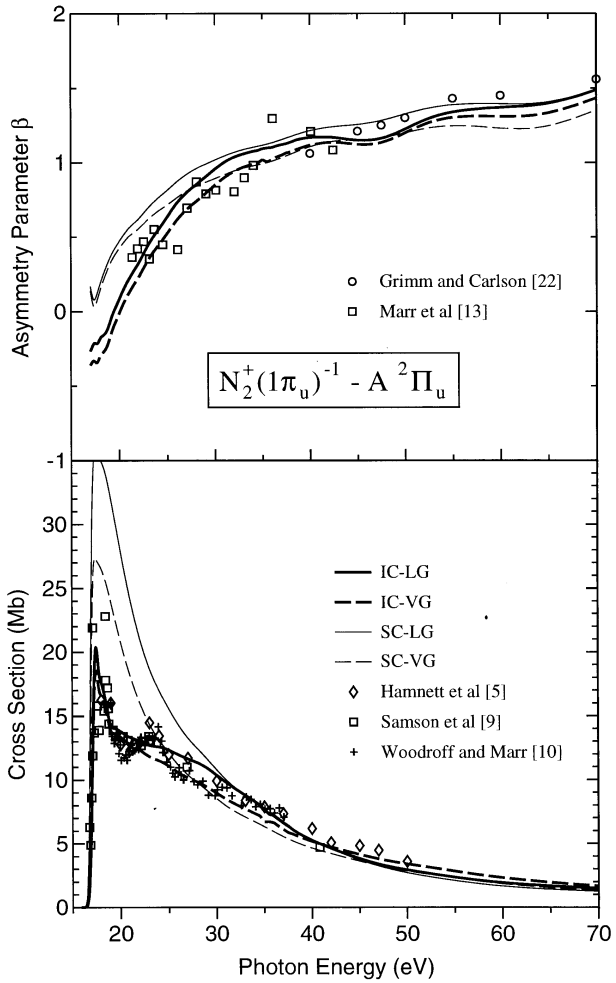

FIG. 4. Partial cross section (Mb) and asymmetry parameter β for the photoionization leading to the $N_2^+(1\pi_u)^{-1}A\ ^2\Pi_u$ state in the 15–70-eV photon energy range. See caption to Fig. 1.

D. Photoionization from the $1\pi_u$

Figure 4 displays the cross section and the asymmetry parameter for the partial photoionization channel involving the $1\pi_u$ orbital, e.g., leading to the $A\ ^2\Pi_u$ ion state.

The partial cross section results are close to those of Lucchese and Zurales [50], and also to the multiconfiguration RPA (MCRPA) results of Swanstrøm *et al.* [46]. The interchannel coupling is of primary importance in order to reach a satisfactory agreement with experiment at least for photon energies up to 30 eV. Also, the spectrum located just above threshold (about 18 eV) is characterized by several Feshbach-type resonances converging to the $2\sigma_u$ threshold, which are quite satisfactorily reproduced by our IC calculations. The SC approximation leads here to a broad and strong peak which is drastically reduced upon introduction of channel coupling, see also Refs. [50, 51].

Some disagreement remains for the structure seen by experimentalists at about 24 eV. Our IC results are of the correct magnitude but smooth down the features of the spectrum.

The differences between SC and IC are less pronounced in the asymmetry parameter (upper part of Fig. 4), and the agreement with experiment is here fairly good everywhere.

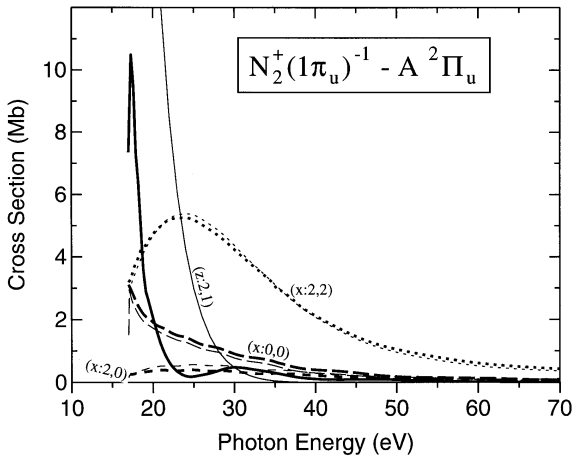

FIG. 5. Absolute contribution of the individual partial wave channels to the photoionization leading to the $N_2^+(1\pi_u)^{-1}A\ ^2\Pi_u$ state. See caption to Fig. 3.

The fine structure predicted in Ref. [51] is absent in our approximation.

At high photon energies (>30 eV) our IC estimate of β is lower than the multichannel frozen core Hartree-Fock estimates of Lucchese and Zurales [50] and much closer to both our and their SC values. Note that the calculation of Ref. [50] gives an autoionizing resonance structure around 38 eV, e.g., where Marr *et al.* [13] observe a peak in the asymmetry parameter. In our calculations the weak Feshbach resonances due to the Rydberg series converging to the $2\sigma_g$ threshold are smoothed down by the convolution procedure.

A detailed analysis of the contribution of each PWC, see Fig. 5, shows the following.

(1) The channel interaction reduces drastically the importance of the $1\pi_u \rightarrow k(2,1)\pi_g$ channel and thus the strength of the partial cross section with respect to SC. The contribution of this channel, whose continuum orbitals mix with the antibonding $1\pi_g^*$ orbital, is very strong in the region around 20 eV but goes to zero rapidly as the photon energy increases. As discussed in Sec. IV A the $^1\Pi_u$ symmetry is much less affected by the channel mixing.

(2) For photon energies larger than 30 eV the partial cross section is dominated by the $1\pi_u \rightarrow k(2,2)\delta_g\ ^1\Pi_u$ PWC (70–80 %), which is very weakly affected by the channel mixing.

E. Photoionization from the $2\sigma_u$

Figure 6 shows our results for the partial photoionization cross section and asymmetry parameter for the $N_2^+(2\sigma_u)^{-1}B\ ^2\Sigma_u^+$ ion state.

Interchannel coupling is particularly important for this channel. The SC and IC curves cross at about 30 eV, with the channel interaction enhancing the cross section below the crossing point and decreasing it beyond. In the low energy region the IC results are in general agreement with the several experimental results. On the other hand, the SC approach furnishes results closer to experiment in the high photon energy region. Our results for the partial cross section are very close to those of Ref. [50]. It should be stressed though that the experimental data taken from different sources show an erratic behavior.

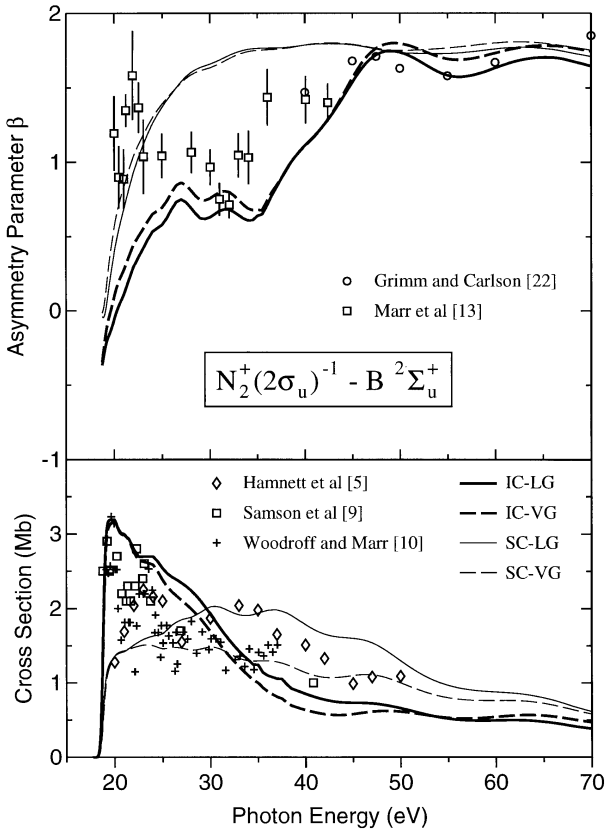

FIG. 6. Partial cross section (Mb) and asymmetry parameter β for the photoionization leading to the $N_2^+(2\sigma_u)^{-1}B\ ^2\Sigma_u^+$ state in the 15–70-eV photon energy range. See caption to Fig. 1.

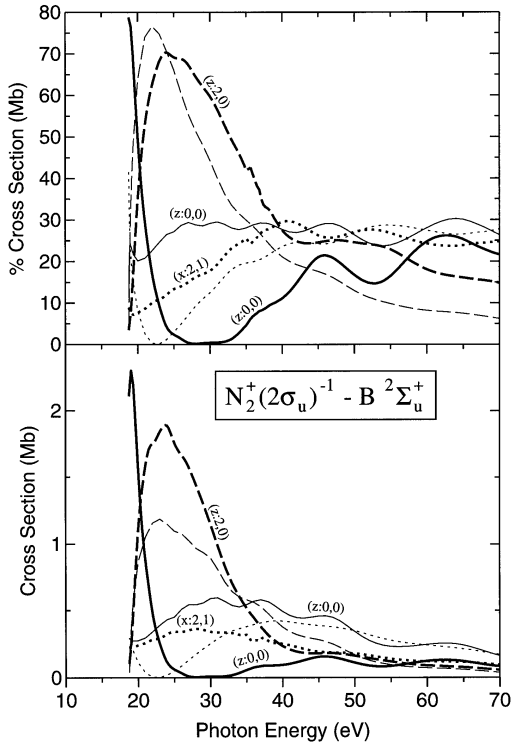

FIG. 7. Contribution of the individual partial wave channels to the photoionization leading to the $N_2^+(2\sigma_u)^{-1}B\ ^2\Sigma_u^+$ state. See caption to Fig. 3.

The increase of the cross section from SC to IC in the 20–25-eV energy range is due to an interaction between the $2\sigma_u \rightarrow k(0,0)\sigma_g$, $2\sigma_u \rightarrow k(2,0)\sigma_g$, and the $1\pi_u \rightarrow k(2,1)\pi_g$ PWC's, with transfer of oscillator strength from the $1\pi_u$ to the $2\sigma_u$ ionization channel. The contribution of the $1\pi_u \rightarrow k(2,1)\pi_g$ PWC to the cross section of N_2 in this region decreases drastically with the introduction of the interchannel coupling, while the oscillator strength of the $3\sigma_g$ and $2\sigma_u$ channels shows a corresponding increase.

To get an insight into this intensity transfer, two *ad hoc* two-channel calculations were performed. The first one, including only the $3\sigma_g$ and $2\sigma_u$ channels, shows the borrowing of oscillator strength from the $2\sigma_u$ to the more intense $3\sigma_g$ channel above 25 eV. The resulting $2\sigma_u$ cross section above 30 eV is similar to the IC results of Fig. 6. A second calculation, taking into account only the $1\pi_u$ and $2\sigma_u$ channels, furnished a larger (4–4.5 Mb) $2\sigma_u$ cross section in the 20–25-eV energy range while no relevant mixing effects were seen above 30 eV. These evidences indicate unambiguously a mechanism of transfer of oscillator strength from the $1\pi_u$ to both the $2\sigma_u$ and $3\sigma_g$ channels, together with the transfer seen from the $2\sigma_u$ to the $3\sigma_g$. For photon energies larger than 30 eV the $1\pi_u$ channel is not practically coupled to the other channels, while the interaction between the $3\sigma_g$ and $2\sigma_u$ persists. Since the $3\sigma_g$ continues to borrow intensity from the $2\sigma_u$ channel, and this action is no longer compensated by the $1\pi_u$ channel, a net decrease of the $2\sigma_u$ partial cross section is observed above 30 eV. The $2\sigma_u$ to $3\sigma_g$ intensity borrowing was shown to persist even when nuclear displacements from the equilibrium geometry are taken into account [49].

A detailed analysis of the contribution of each PWC (Fig. 7) confirms these very strong mixing effects and allows further scrutiny of the intrachannel mechanisms.

The (2,1) PWC shows in the SC approximation at $\sim$23 eV a Cooper minimum which disappears in the IC case. On the contrary the (0,0) PWC shows a minimum around 30 eV only in the IC case. A comparison of the PWC contributions to the $2\sigma_u$ cross section of Fig. 7 with those arising from the two-channel calculations leads to the following conclusions.

(1) The (0,0) PWC is involved in the $2\sigma_u - 3\sigma_g$ interaction and it accounts for the decrease of the $2\sigma_u$ cross section. In the 18–30-eV region this PWC interacts also with the $1\pi_u$ channel, from which it borrows intensity.

(2) The (2,0) PWC receives the $1\pi_u$ intensity and it accounts for the increase of the $2\sigma_u$ cross section in the 20–30-eV range.

(3) The (2,1) PWC (of $^1\Pi_u$ symmetry) is involved in the $2\sigma_u - 3\sigma_g$ interaction and it is less affected by the $2\sigma_u - 1\pi_u$ interaction. This PWC works together with the (0,0) PWC in the high energy region of the spectrum to decrease the $2\sigma_u$ cross section going from SC to IC.

There are some uncertainties both in the *ab initio* results and in the experiment concerning the behavior of the $2\sigma_u$ partial cross section in the 30-eV photon energy region. Experimental results are not well resolved and conflicting. Hamnett, Stoll, and Brion [5] find a broad maximum around

34 eV, Plummer *et al.* [11] and Woodruff and Marr [10] both find a sequence of small minima and maxima, located in some instances at different photon energies. All our data point to the evidence that the cross section decreases steadily as the photon energy increases. This is in agreement with Lucchese and Zurales [50], but not with Stephens and Dill [45], who apparently observed a steady increase.

The experimental asymmetry parameter shows a broad valley around 30 eV, due again to the interaction with the $3\sigma_g \rightarrow \sigma_u$ shape resonance. Only vibrationally averaged experimental data are shown in Fig. 6. As expected, the theoretical β shows a remarkable dependence on the interchannel coupling up to photon energies of the order of 50 eV. The two experimental maxima around 22 eV—due probably to doubly excited states—are not reproduced by our approximations. Our IC asymmetry parameter in the 20–25-eV region is also smaller than the results of Lucchese and Zurales [50]. See also [51].

The two-channel calculation ($3\sigma_g$ plus $2\sigma_u$) gives results for β which agree very well with the experimental data (value of ~ 1) for photon energies greater than 25 eV and with the exception of the narrow region around 30 eV where the deep is seen [13]. The further introduction of the coupling with the $1\pi_u$ channel decreases β by about 0.2–0.3 in the 25–35-eV energy range. Since the two-channel ($1\pi_u$ plus $2\sigma_u$) calculation furnishes an asymmetry parameter which is increasing in this region and gives no sign of a plateau, it seems that the behavior seen in Fig. 6 is the result of the strong and complex three-channel interaction just discussed.

F. Photoionization from the $2\sigma_g$

Figure 8 displays the cross section and the asymmetry parameter for the partial photoionization channel leading to the $(2\sigma_g)^{-1}\ ^2\Sigma_g^+$ ion state.

The inner-valence-photoelectron spectrum of N_2 in the 36–40-eV photon energy range shows a complex structure [18,22] which has been attributed [39] essentially to the interaction of the $(2\sigma_g)^{-1}\ ^2\Sigma_g^+$ ion state with outer-valence excited ion states occurring in the same energy range. As well as for inner-valence ionization of other molecules [67], in spite of the inadequacy of the one-electron picture and Koopman's theorem in this region, the RPA is still justified. In fact the intensity of these multiplets for molecules whose ground state can be described to a good approximation by a single configuration comes mainly from the singly excited configurations with an inner-valence hole. Thus our approximation reduces the complex structure to a single peak. Beyond 40 eV the calculated observables may be reasonably compared with experiment. Note that the $2\sigma_g$ ionization threshold was chosen to be at 38 eV, which roughly corresponds to the centroid of these multiplets [18,51]. Support to our hypothesis comes from the evident agreement of our cross section with that computed by Langhoff *et al.*, obtained summing the contributions from the several peaks in the 30–40-eV region [39].

Both the partial cross section and the asymmetry parameter are in satisfactory agreement with experiment. As expected for photoionization from inner-valence orbitals, the effect of the channel mixing is small, due to the remarkable

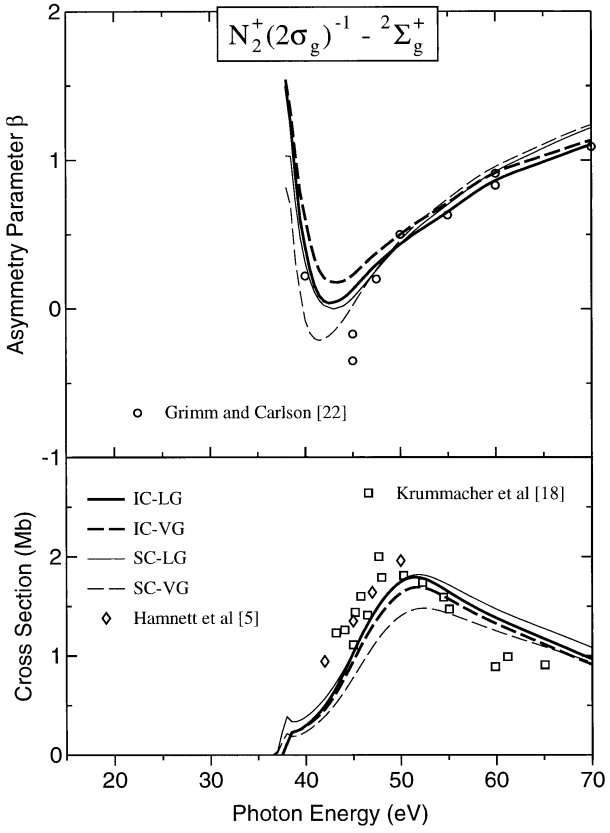

FIG. 8. Partial cross section (Mb) and asymmetry parameter β for the photoionization leading to the $N_2^+(2\sigma_g)^{-1}\ ^2\Sigma_g^+$ state in the 15–70-eV photon energy range. See caption to Fig. 1.

energy differences in the waves involved in the Hamiltonian matrix elements at a given energy.

At about 13–14 eV above threshold, the $2\sigma_g$ partial cross section exhibits a shape resonant peak. In this region (~ 50 eV) the contribution of the (3,0) wave has a neat maximum analogous to that seen for the shape resonance discussed for the $3\sigma_g$ channel in Sec. IV C.

The more interesting feature of the asymmetry parameter is the broad deep around 5 eV above threshold. At very low photoelectron energies the entire contribution to the partial cross section is given by the (1,0) and $(1,\pm 1)$ PWC's but, as the energy increases, the contribution of the (3,0) PWC becomes larger, overcoming that of the p PWC's quite rapidly. This rearrangement is responsible for the dramatic variation of the angular distribution in the 43-eV region.

V. CONCLUSIONS

We performed a detailed study of the features of the photoelectron spectrum of molecular nitrogen. We employed the K-matrix L^2 approach which we have experimented with successfully in the last decade, and exploited the advantages given by the use of Gaussian-type orbitals for the description of the continuum partial waves. An analysis of the effect of interchannel coupling on the total and partial cross section and asymmetry parameter, including all four valence ionization channels, was carried out.

The major features of the photoelectron spectrum of N_2

were recovered. The technique allowed us to study in some detail the interplay of multichannel effects on the shape resonances and the subtleties of the intensity borrowing phenomena, especially evident in this system. A detailed analysis of the effect of the localized channel in the expansion basis for the continuum was made: its presence has an appreciable effect on the property under study. Also, we proved that the extension of the angular moment quantum number of the partial wave channels up to $l=7$ is sufficient to obtain stable results.

Our study does not include the effect of electron correlation on the ion state as done recently (for the 19–26-eV photon energy range) by Stratmann, Bandarage, and Lucchese [51] with a multichannel configuration interaction approach or by Swanstrøm *et al.* [46] employing MCRPA. Also, the effects of the relaxation of the fixed nuclei approximation, which Basden and Lucchese proved to be quite important at least to explain some of the features of the spectrum [49], are not considered here. We extended, on the other hand, our analysis to the inner-valence $2\sigma_g$ orbital.

The study of the photoelectron spectrum of nitrogen can be considered a classic test for the theoretical approaches to the description of molecular continuum. We believe that the K-matrix L^2 approach coupled to the use of extended spherical polynomial GTO-type orbitals has shown its capability for the purpose of describing in good detail the complex features of the total and differential cross section of N_2. Our previous studies with the same approach [62,63] concerned relatively simple (H_2 [62], Li_2, LiH [63]) systems. The present work leaves us confident that, with the rapid increase in computational power, we should soon be able to take the study of continuum properties to the realm of larger molecular systems.

ACKNOWLEDGMENT

One of the authors (R.M.) acknowledges the financial support of the Italian Consiglio Nazionale delle Ricerche.

[1] D. R. Denne, J. Phys. D **3**, 1392 (1970).
[2] T. M. El-Sherbini and M. J. van der Wiel, Physica (Amsterdam) **59**, 433 (1972).
[3] W. S. Watson, J. Lang, and D. T. Stewart, J. Phys. B **6**, L148 (1973).
[4] L. C. Lee, R. W. Carlson, D. L. Judge, and M. Ogawa, J. Quant. Spectrosc. Radiat. Transfer **13**, 1023 (1973).
[5] A. Hamnett, W. Stoll, and C. E. Brion, J. Electron Spectrosc. Relat. Phenom. **8**, 367 (1976).
[6] G. R. Wight, M. J. Van der Wiel, and C. E. Brion, J. Phys. B **9**, 675 (1976).
[7] P. Gürtler, V. Saile, and E. E. Koch, Chem. Phys. Lett. **48**, 245 (1977).
[8] L. De Reilhac and N. Damany, J. Quant. Spectrosc. Radiat. Transfer **18**, 121 (1977).
[9] J. A. R. Samson, G. N. Haddad, and J. L. Gardner, J. Phys. B **10**, 1749 (1977).
[10] P. R. Woodruff and G. V. Marr, Proc. R. Soc. London, Ser. A **358**, 87 (1977).
[11] E. W. Plummer, T. Gustafsson, W. Gudat, and D. E. Eastman, Phys. Rev. A **15**, 2339 (1977).
[12] B. E. Cole and R. N. Dexter, J. Phys. B **11**, 1011 (1978).
[13] G. V. Marr, J. M. Morton, R. M. Holmes, and D. G. McCoy, J. Phys. B **12**, 43 (1979).
[14] S. Wallace, D. Dill, and J. L. Dehmer, J. Phys. B **12**, L417 (1979).
[15] J. B. West, A. C. Parr, B. E. Cole, D. L. Ederer, R. Stockbauer, and J. L. Dehmer, J. Phys. B **13**, L105 (1980).
[16] R. M. Holmes and G. V. Marr, J. Phys. B **13**, 945 (1980).
[17] T. A. Carlson, M. O. Krause, D. Mehaffy, J. W. Taylor, F. A. Grimm, and J. D. Allen, Jr., J. Chem. Phys. **73**, 6056 (1980).
[18] S. Krummacher, V. Schmidt, and F. Wuilleumier, J. Phys. B **13**, 3993 (1980).
[19] M. O. Krause, T. A. Carlson, and P. R. Woodruff, Phys. Rev. A **24**, 1374 (1981).
[20] J. B. West, K. Codling, A. C. Parr, D. L. Ederer, B. E. Cole, R. Stockbauer, and J. L. Dehmer, J. Phys. B **14**, 1791 (1981).
[21] P. Morin, M. Y. Adam, I. Nenner, J. Delwiche, M. J. Hubin-Franskin, and P. Lablanquie, Nucl. Instrum. Methods Phys. Res. **208**, 761 (1983).
[22] F. A. Grimm and T. A. Carlson, Chem. Phys. **80**, 389 (1983).
[23] S. H. Southworth, A. C. Parr, J. E. Hardis, and J. L. Dehmer, Phys. Rev. A **33**, 1020 (1986).
[24] E. D. Poliakoff, M. Ho, G. E. Leroi, and M. G. White, J. Chem. Phys. **84**, 4779 (1986).
[25] J. A. R. Samson, T. Masuoka, P. N. Pareek, and G. C. Angel, J. Chem. Phys. **86**, 6128 (1987).
[26] M. Ukai, K. Kameta, N. Kouchi, and Y. Hatano, Phys. Rev. A **46**, 7019 (1992).
[27] E. D. Poliakoff, S. Kahar, and R. A. Rosenberg, J. Chem. Phys. **96**, 2740 (1992).
[28] P. Erman, A. Karawajczyk, U. Köble, E. Rachlew, K. Yoshiki Franzén, and L. Veseth, Phys. Rev. Lett. **76**, 4136 (1996).
[29] A. Temkin and K. V. Vasavada, Phys. Rev. **160**, 109 (1967).
[30] J. L. Dehmer and D. Dill, Phys. Rev. Lett. **35**, 213 (1975).
[31] J. L. Dehmer and D. Dill, J. Chem. Phys. **65**, 5327 (1976).
[32] J. W. Davenport, Phys. Rev. Lett. **36**, 945 (1976).
[33] C. Duzy and R. S. Berry, J. Chem. Phys. **64**, 2421 (1976).
[34] J. W. Davenport, Int. J. Quantum Chem. Quantum Biol. Symp. **11**, 89 (1977).
[35] T. N. Rescigno, C. F. Bender, B. V. McKoy, and P. W. Langhoff, J. Chem. Phys. **68**, 970 (1978).
[36] T. N. Rescigno, A. Gerwer, B. V. McKoy, and P. W. Langhoff, Chem. Phys. Lett. **66**, 116 (1979).
[37] F. Hirota, Chem. Phys. Lett. **74**, 67 (1980).
[38] G. Raseev, H. Le Rouzo, and H. Lefebvre-Brion, J. Chem. Phys. **72**, 5701 (1980).
[39] P. W. Langhoff, S. R. Langhoff, T. N. Rescigno, J. Schirmer, L. S. Cederbaum, W. Domcke, and W. von Niessen, Chem. Phys. **58**, 71 (1981).
[40] G. R. J. Williams and P. W. Langhoff, Chem. Phys. Lett. **78**, 21 (1981).
[41] R. R. Lucchese, G. Raseev, and V. McKoy, Phys. Rev. A **25**, 2572 (1982).

[42] M. Raoult, H. Le Rouzo, G. Raseev, and H. Lefebvre-Brion, J. Phys. B **16**, 4601 (1983).
[43] Z. H. Levine and P. Soven, Phys. Rev. A **29**, 625 (1984).
[44] L. A. Collins and B. I. Schneider, Phys. Rev. A **29**, 1695 (1984).
[45] J. A. Stephens and D. Dill, Phys. Rev. A **31**, 1968 (1985).
[46] P. Swanstrøm, J. T. Golab, D. L. Yeager, and J. A. Nichols, Chem. Phys. **110**, 339 (1986).
[47] B. Basden and R. R. Lucchese, Phys. Rev. A **34**, 5158 (1986).
[48] S. Yabushita, C. W. McCurdy, and T. N. Rescigno, Phys. Rev. A **36**, 3146 (1987).
[49] B. Basden and R. R. Lucchese, Phys. Rev. A **37**, 89 (1988).
[50] R. R. Lucchese and R. W. Zurales, Phys. Rev. A **44**, 291 (1991).
[51] R. E. Stratmann, G. Bandarage, and R. R. Lucchese, Phys. Rev. A **51**, 3756 (1995).
[52] J. W. Gallagher, C. E. Brion, J. A. R. Samson, and P. W. Langhoff, J. Phys. Chem. Ref. Data **17**, 9 (1988).
[53] J. C. Slater and K. H. Johnson, J. Phys. B **5**, 844 (1972).
[54] P. W. Langhoff, in *Electron Molecule and Photon Molecule Collisions*, edited by T. Rescigno, B. McKoy, and B. Schneider (Plenum, New York, 1979), p. 183.
[55] P. W. Langhoff, in *Theory and Application of Moment Methods in Many-Fermions Systems*, edited by B. Dalton, S. Grimes, J. Vary, and S. Williams (Plenum, New York, 1980), p. 191.
[56] R. R. Lucchese, D. K. Watson, and V. McKoy, Phys. Rev. A **22**, 421 (1980).
[57] R. R. Lucchese, K. Takatsuka, D. K. Watson, and V. McKoy, in *Proceedings of the Symposium on Electron-Atom and Molecule Collisions*, edited by U. Bielefeld (Plenum, London, 1981), p. 191.
[58] I. Cacelli, V. Carravetta, A. Rizzo, and R. Moccia, in *Modern Techniques in Computational Chemistry: MOTECC-90*, edited by E. Clementi (Escom, Leiden, 1990), p. 639.
[59] I. Cacelli, V. Carravetta, A. Rizzo, and R. Moccia, Phys. Rep. **205**, 283 (1991).
[60] I. Cacelli, V. Carravetta, A. Rizzo, and R. Moccia, in *Applied Many-Body Methods in Spectroscopy and Electronic Structure*, edited by D. Mukherjee (Plenum, New York, 1992), p. 105.
[61] I. Cacelli, V. Carravetta, and R. Moccia, J. Chem. Phys. **85**, 7038 (1986).
[62] I. Cacelli, R. Moccia, and A. Rizzo, J. Chem. Phys. **98**, 8742 (1993).
[63] I. Cacelli, R. Moccia, and A. Rizzo, J. Chem. Phys. **102**, 7131 (1995).
[64] A. Rizzo, MCENTER (unpublished).
[65] U. Fano, Phys. Rev. **124**, 1866 (1961).
[66] R. R. Lucchese, K. Takatsuka, and V. McKoy, Phys. Rep. **131**, 147 (1986).
[67] I. Cacelli, V. Carravetta, and R. Moccia, Chem. Phys. **184**, 213 (1994).
[68] K. P. Huber and G. Herzberg, *Molecular Spectra and Molecular Structure. IV. Constants of Diatomic Molecules* (Van Nostrand Reinhold, New York, 1979).
[69] M. J. Frisch, G. W. Trucks, H. B. Schlegel, P. M. W. Gill, B. G. Johnson, M. A. Robb, J. R. Cheeseman, T. A. Keith, G. A. Petersson, J. A. Montgomery, K. Raghavachari, M. A. Al-Laham, V. G. Zakrzewski, J. V. Ortiz, J. B. Foresman, J. Cioslowski, B. B. Stefanov, A. Nanayakkara, M. Challacombe, C. Y. Peng, P. Y. Ayala, W. Chen, M. W. Wong, J. L. Andres, E. S. Replogle, R. Gomperts, R. L. Martin, D. J. Fox, J. S. Binkley, D. J. Defrees, J. Baker, J. P. Stewart, M. Head-Gordon, C. Gonzalez, and J. A. Pople, GAUSSIAN 94 (Revision A.1) (Gaussian, Inc., Pittsburgh, PA, 1995).
[70] D. W. Turner, C. Baker, A. D. Baker, and R. C. Brundle, *Molecular Photoelectron Spectroscopy* (Wiley, New York, 1970).
[71] J. J. Hopfield, Phys. Rev. **36**, 789 (1930).
[72] I. Cacelli and V. Carravetta, Chem. Phys. **204**, 89 (1996).
[73] I. Cacelli and R. Moccia, Int. J. Quantum Chem. **60**, 409 (1996).
[74] R. Moccia and P. Spizzo, Can. J. Chem. **70**, 513 (1992).
[75] J. L. Gardner and J. A. R. Samson, J. Chem. Phys. **62**, 1447 (1975).